JOC The Journal of Organic Chemistry

Article

pubs.acs.org/joc

Structure and Photochemistry of a Saccharyl Thiotetrazole

A. Ismael,[†,‡] A. Borba,[‡] M. S. C. Henriques,[§] J. A. Paixão,[§] R. Fausto,*[,‡] and M. L. S. Cristiano*[,†]

[†]CCMAR and Department of Chemistry and Pharmacy, F.C.T., University of Algarve, P-8005-039 Faro, Portugal

[‡]Department of Chemistry, University of Coimbra, P-3004-535 Coimbra, Portugal

[§]CEMDRX, Department of Physics, University of Coimbra, P-3004-516 Coimbra, Portugal

Supporting Information

ABSTRACT: The molecular structure and photochemistry of 5-thiosaccharyl-1-methyltetrazole (TSMT) were studied by means of matrix-isolation FTIR spectroscopy, X-ray crystallography, and theoretical calculations. The calculations predicted two conformers of TSMT that differ in energy by more than 15 kJ mol^{-1}. The infrared spectrum of TSMT isolated in solid argon was fully assigned on the basis of the spectrum calculated (O3LYP/6-311++G(3df,3pd)) for the most stable conformer. In the crystal, TSMT molecules were found to assume the same conformation as for the isolated molecule, with each molecule forming four hydrogen bonds with three neighboring molecules, leading to a network of TSMT oligomers. Upon UV (λ = 265 nm) irradiation of the matrix-isolated TSMT, two photodegradation pathways were observed, both arising from cleavage of the tetrazolyl ring. Pathway *a* involves cleavage of the N_1-N_2 and N_3-N_4 bonds with extrusion of N_2, leading to photostable diazirine and thiocarbodiimide derivatives. The photostability of the photoproduced diazirine under the conditions used precluded its rearrangement to the nitrile imine, as reported for 5-phenyltetrazole by Bégué et al. (*J. Am. Chem. Soc.* **2012**, *134*, 5339). Pathway *b* involves cleavage of the C_5-N_1 and N_4-N_3 bonds, leading to a thiocyanate and methyl azide, the latter undergoing subsequent fragmentation to give CNH.

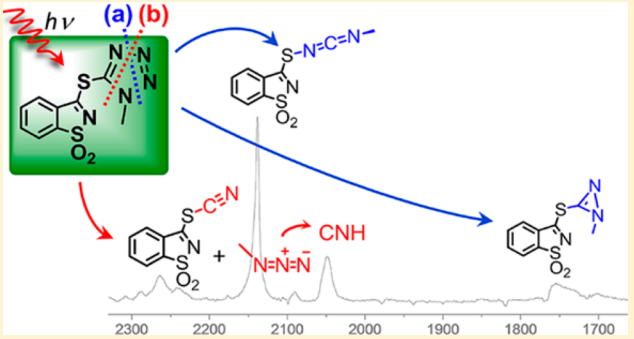

INTRODUCTION

Derivatives of the heterocycles tetrazole and saccharin are widely applied in coordination chemistry as ligands.[1,2] Tetrazole can coordinate through four electron-donating nitrogen atoms and may therefore act as a multidentate ligand or as a bridging building block in supramolecular assemblies. It has the potential to participate in seven distinct types of coordination modes with metal ions, and therefore, tetrazole-based coordination compounds are used in catalysis and in the construction of metal−organic frameworks.[3−6] Similarly, saccharin and the saccharinate anion (1,2-benzisothiazole-3-one-1,1-dioxide anion; deprotonated saccharin) interact with metal centers in various ways, generating relatively strong interactions in crystalline environments, mostly through hydrogen bonding. As a polyfunctional ligand, saccharin can be engaged in N−, O(C═O)−, or O(SO_2)−metal coordination and can also act as a bidentate amidato-like bridging agent.[7−9] On the basis of the structural features and coordination capabilities of both heterocycles, we envisaged investigating the potential of saccharyl−tetrazole conjugates (Figure 1) as bridging ligands. Synthetic routes to a small library of these target compounds were devised and optimized[10] in view of exploring their application as coordination ligands for transition metals.

Understanding the relevance of different tautomeric forms and preferred conformations of chemical systems is instrumental in predicting and exploring their properties and function. As such, the structure of selected saccharyl−tetrazole conjugates was investigated in detail both in the isolated molecule situation, by matrix-isolation infrared spectroscopy and contemporary methods of quantum chemistry, and in the neat crystalline phase, by X-ray crystallography and infrared and Raman spectroscopies.[11,12] Among the conjugates investigated, nitrogen-linked saccharinate tetrazoles (Figure 1; X = NH) proved especially challenging because of the possibility of tautomerism involving the saccharyl system.[11,12] For these compounds, two forms are possible: the iminosaccharin and aminosaccharin tautomers. If, additionally, the tetrazole ring is unsubstituted (Figure 1; X = NH, R = H), as is the case for *N*-

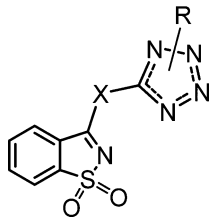

Figure 1. General structure of the saccharyl−tetrazole conjugates.

Received: October 22, 2014
Published: December 1, 2014

(1,1-dioxo-1,2-benzisothiazol-3-yl)amine-1*H*-tetrazole,[11] then four tautomers become possible, two belonging to the iminosaccharin group and the other two to the aminosaccharin group. We found that the amino-linked conjugates may exhibit different structures in the crystalline and gaseous phases.[11,12] On the contrary, for a thio-linked saccharyl tetrazole such as the title compound, the structure simplifies because of the absence of tautomerism involving the saccharyl system. In addition, the possibility of tautomerism involving the tetrazole ring may be quenched through the introduction of a suitable substituent. Here we describe the synthesis and detailed structural analysis of 1,2-benzisothiazole-1,1-dioxo-3-(5-thio-1-methyl)tetrazole (5-thiosaccharyl-1-methyltetrazole, TSMT, **3**) (Scheme 1) in the crystalline state and in solid argon.

Scheme 1. Synthetic Approach to 5-Thiosaccharyl-1-methyltetrazole (TSMT)

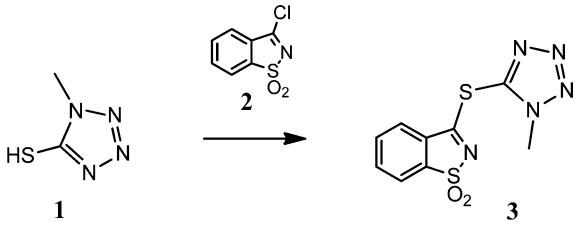

When considering applications of saccharyl−tetrazole conjugates, assessment of photostability may be a relevant aspect. In general, the benzisothiazole moiety is known to be rather photostable compared with the tetrazole moiety. The photochemistry of monomeric saccharin isolated in solid argon was recently investigated.[13] A search in the literature also yielded some data regarding the photochemistry of some benzisothiazoles in solution,[14−23] indicating that the photoreactivity is determined by the structure of the saccharyl ring, the nature of substituents, and the reaction medium. By their turn, tetrazoles are known for their rich photochemistry both in solution and isolated in cryogenic matrices.[24,25] Generally, the photochemistry of tetrazole derivatives is influenced by the chemical nature and conformational flexibility of substituents, and when the molecule exhibits tautomerism, tautomer-selective photochemistry may take place.[25,26]

The fact that tetrazole−saccharyl conjugates combine heterocyclic moieties with dissimilar intrinsic photoreactivities is challenging and provides yet another reason to explore the photoreactivity of benzisothiazolyl−tetrazole conjugates by matrix-isolation FTIR spectroscopy. This method offers several advantages for studying the photochemistry of monomeric compounds (i.e., molecular diffusion is inhibited, leading—in principle—only to the observation of unimolecular reactions and enabling the stabilization, detection, and characterization of products and in some cases intermediates).[25]

Here we report on the UV-induced photochemistry of TSMT in solid argon. As mentioned above, in this saccharyl−tetrazole conjugate the methyl substituent on the tetrazole ring quenches the possibility of tautomerism involving the tetrazole and the thioether linkage restricts tautomerism involving the saccharyl system, thus reducing the number of structures present in the matrix and simplifying the interpretation of the photochemical reactions. Interpretation of the experimental results is assisted by quantum-chemical calculations undertaken at different levels of approximation.

RESULTS AND DISCUSSION

Geometries and Energies of TSMT. TSMT has two intramolecular rotational degrees of freedom, represented by arrows in Figure 2, which may result in different conformers.

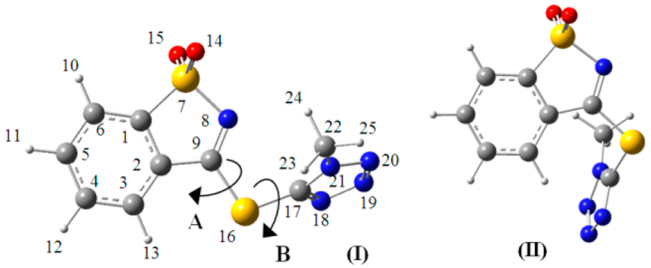

Figure 2. Optimized structures of the theoretically predicted conformers of TSMT. The atom numbering adopted is shown. Arrows A and B relate to the two conformationally relevant degrees of freedom.

These are related to the orientations of the saccharyl and tetrazolyl rings relative to the C−S−C plane (dihedral angles A and B, respectively).

To identify the minimum-energy conformations of TSMT, a systematic investigation of the potential energy surface (PES) of the molecule was undertaken using the B3LYP/6-31++G(d,p) method. The locations of the minima on the bidimensional PES map obtained by performing relaxed scans on the PES are shown in Figure 3. In building this map, dihedral angles A (N_8−C_9−S_{16}−C_{17}) and B (C_9−S_{16}−C_{17}−N_{18}) were varied in increments of 30°, while all of the other geometric parameters were let free during the geometry

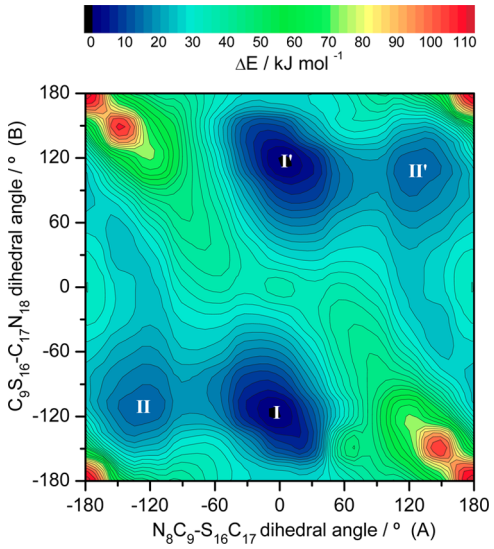

Figure 3. Potential energy surface map of TSMT calculated at the B3LYP/631++G(d,p) level of theory as a function of the dihedral angles A (N_8−C_9−S_{16}−C_{17}) and B (C_9−S_{16}−C_{17}−N_{18}). These two dihedral angles were incrementally fixed with a step of 30° while the remaining parameters were let free during geometry optimization. The positions of the two conformers are shown in the graph by their numbers, I and II. Each of these minima belongs to the C_1 symmetry point group and has a symmetry-equivalent counterpart, also presented in the graph with primes, I′ and II′. The electronic energy of form I was chosen as the relative zero. See Figure 2 for structures and atom numbering.

dx.doi.org/10.1021/jo502419u | *J. Org. Chem.* 2015, 80, 392−400

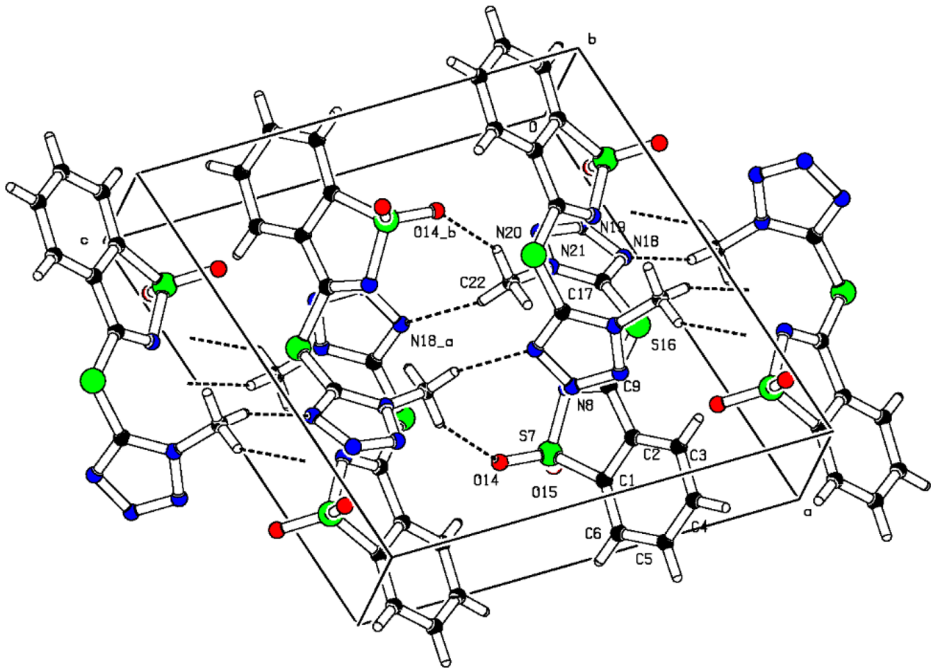

Figure 4. Hydrogen-bonding network in the crystal of TSMT. The ORTEPII plot showing the geometry of the TSMT molecule in the crystal is provided in Figure S1 in the Supporting Information and closely resembles the theoretically predicted conformer I.

optimization. According to the calculations, TSMT may exist in two different conformers (I and II; Figure 2). The full geometry optimization of the two conformers was carried at the O3LYP/6-311++G(3df,dpd) level of theory. The O3LYP hybrid functional was selected for these calculations because it has been shown to constitute an improvement over the B3LYP one,[27] particularly in the prediction of geometries and infrared spectra of derivatives of saccharin.[13] Geometrical parameters are provided in Computational Data in the Supporting Information.

In the more stable conformer, I, the tetrazole ring is considerably rotated in relation to the C−S−C plane (i.e., B = ±115° in the two symmetry-equivalent minima corresponding to this conformer; see Figure 3), while the dihedral angle A is close to 0° (i.e., the plane of the saccharyl moiety is nearly aligned with the C−S−C plane, with the C═N bond eclipsing the S_{16}−C_{17} bond). It should be noted that the structures with C_s symmetry, in which the tetrazolyl and saccharyl groups are coplanar (A = 0°, B = 0° and A = 0°, B = 180°), are destabilized by steric repulsions between the closely located N_{18} and N_8 lone-electron pairs and the CH_3 group and N_8 lone pair, respectively. In conformer I, a stabilizing interaction occurs between the nitrogen atom of the saccharyl moiety and the hydrogen of the methyl group because in the minimum-energy geometry the distance between these atoms and their relative orientation fit well the requirements for an attractive interaction (weak C−H···N hydrogen-bond-like interaction). In addition, electronic delocalization involving the lone pairs of electrons on the sulfur atom and the π systems of the rings also contribute to determine this conformational preference.

The energy of conformer II was predicted to be 15 kJ mol^{-1} higher than that of conformer I. Conformer II differs from conformer I by internal rotation about the C_9−S_{16} bond (i.e., A = ±137°). In this conformer, a weak stabilizing intramolecular interaction of the C−H···N type is present between nitrogen atom N_{18} of the tetrazole ring and hydrogen atom H_{13} of the phenyl ring (see Figure 2). The calculated barrier for isomerization of the higher-energy conformer II into the more stable conformer I is 6.1 kJ mol^{-1} (19.4 kJ mol^{-1} in the reverse direction; for coordinates of the transition-state structure, see Computational Data in the Supporting Information). According to the calculated energy difference between II and I, the population of conformer II in the gas phase at room temperature (25 °C) is only 0.2%; at the temperature used to prepare the matrices of the compound in the present investigation (100 °C), it is still below 1%. One can then anticipate that only conformer I might be trapped from the gas phase into the deposited cryogenic matrices.

Crystal Structure of TSMT and IR Spectrum of the Crystal. The structure of crystalline TSMT, determined by X-ray analysis, is provided in Figure 4 (packing diagram) and Figure S1 in the Supporting Information (structure of the monomeric unit in the crystal). Atomic coordinates, bond lengths, valence angles, dihedral angles, and other crystallographic data were deposited at the Cambridge Crystallographic Data Centre with the reference CCDC 1025233.

In the crystal, TSMT exists in the more stable conformation predicted for the isolated molecule (compare Figures 2 and S1). Each molecule is involved in four weak hydrogen bonds with three neighboring molecules. The methyl substituent on the tetrazolyl ring establishes two intermolecular hydrogen bonds with two neighboring molecules, one with a nitrogen atom at position 4 of the tetrazole ring (N_{18}) in the first molecule and another with an oxygen atom of the SO_2 group of the saccharyl system (O_{14}) in the second molecule as acceptors. This same molecule establishes a third intermolecular hydrogen bond through O_{14} of the SO_2 group with the methyl substituent of the previous "second" neighbor and a fourth hydrogen bond with a third neighbor molecule in which N_{18} acts as the acceptor. In addition to these four intermolecular hydrogen bonds, a weak intramolecular interaction can also be considered between the third H atom of the methyl group and the S atom.

dx.doi.org/10.1021/jo502419u | J. Org. Chem. 2015, 80, 392−400

The hydrogen-bonding scheme is shown in Figure 4, and the symmetry-unique short contacts are $C_{22}H_{24}\cdots N_{18}{}^{a}$ (3.486(2) Å), $C_{22}H_{25}\cdots O_{14}{}^{b}$ (3.345(2) Å), and $C_{22}H_{23}\cdots S_{16}$ (3.323(2) Å), where the superscripts "a" and "b" designate atoms belonging to neighboring molecules generated by the symmetry operations a (x, $^1/_2 - y$, $^1/_2 + z$) and b ($1 - x$, $1 - y$, $1 - z$), respectively. This hydrogen-bonding pattern leads to the formation of TSMT oligomers. The oligomeric structure is formed from dimers of TSMT. In each dimer, the two molecules of TSMT are disposed in a head-to-tail arrangement, with the tetrazole moiety of one molecule overlapping the thioimino moiety of the other at the inner part of the dimer while the carbocyclic aromatic rings are directed to the extremities. The oligomeric structure results from an intricate network of weak hydrogen bonds formed between consecutive dimers (with involvement of both molecules of the dimer) and adjacent dimers. Weak $\pi-\pi$ interactions between tetrazole rings and thioimino moieties as well as S−O$\cdots\pi$ interactions (short contacts of 4.65 and 3.01 Å, respectively) may also play a role in the stabilization of the observed supramolecular structure.

A comparison between the geometrical parameters of TSMT monomer I, calculated at the O3LYP/6-311++G(3df,3pd) level of theory, and those determined for the compound in the crystal (Table S1 in the Supporting Information) reveals an excellent correlation between the two sets of data, although in the crystal the dihedral angles A and B (see Figure 2) appear slightly rotated (i.e., A = −10.5° and B = −108.8°) relative to those obtained from theory for the isolated molecule (A = −3.3° and B = −115.3°) as a result of the intermolecular interactions.

The infrared spectrum of neat crystalline TSMT at room temperature is provided in Figure S2 in the Supporting Information. The calculated spectrum of conformer I is also shown in this figure for comparison. Proposed assignments of the spectra are given in Table S2 in the Supporting Information. The good general description of the experimental spectrum of the crystal by the calculated spectrum of the isolated monomer is an indication that the intermolecular interactions present in the solid do not substantially perturb the intramolecular potential.

Infrared Spectra of Matrix-Isolated TSMT. As described in the Experimental Section, a sample of crystalline TSMT was sublimed in vacuo (at ∼100 °C), the vapors of the compound were mixed with argon (ca. 1:1000 molar ratio), and the mixture was deposited onto a substrate kept at 15 K. Figure 5 shows the infrared spectrum of TSMT isolated in an argon matrix prepared in this way. The detailed analysis of the spectrum of matrix-isolated TSMT doubtlessly shows that only conformer I is present in the matrix, as anticipated taking into account the predicted relative energies of the two conformers and their estimated populations in the gas-phase equilibrium before deposition. This is particularly noticeable in the low-frequency region, where according to the calculations the spectra of the two conformers are clearly differentiable (see Figure 6).

UV-Induced Photochemistry of Matrix-Isolated TSMT. In order to investigate the photochemical reactions of TSMT, the deposited matrix was irradiated with UV light, as described in Experimental Section. The sample was monitored after each irradiation by recording its infrared spectrum. The wavelengths used for irradiation were chosen according to the UV−vis spectrum of TSMT in ethanol at room temperature, which shows an absorption maximum at 263 nm.

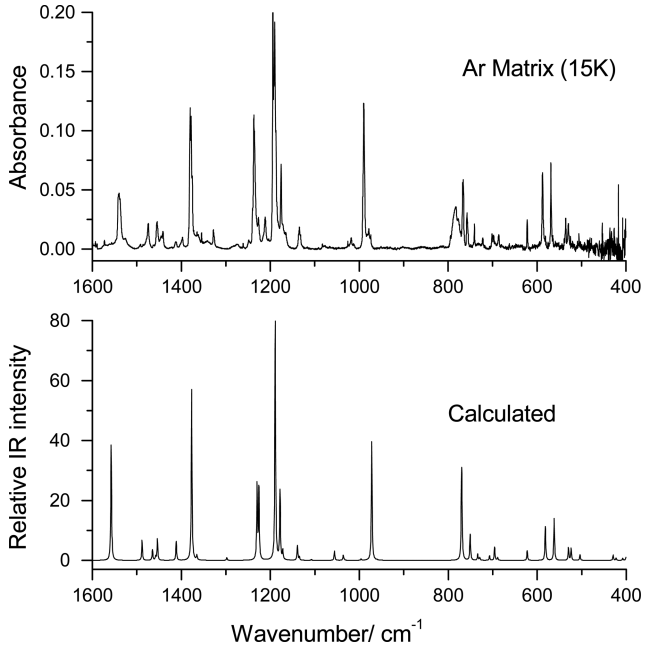

Figure 5. Infrared spectrum of matrix-isolated TSMT (Ar matrix, 15 K) and O3LYP/6-311++G(3df,3pd)-calculated infrared spectrum for the more stable conformer. The calculated spectra were simulated using Lorentzian functions centered at the calculated frequency scaled by 0.992 and with full width at half-maximum (fwhm) equal to 2 cm^{-1}. It should also be noted that the peak intensities in the calculated spectrum differ from the calculated intensity values; in the figure the calculated intensities correspond to the areas of the peaks.

Upon irradiation at 265 nm, the bands due to TSMT decreased in intensity, indicating that the compound was being consumed, and simultaneously, new bands due to photo-produced species appeared in the spectrum. The changes are particularly noticeable in the 2300−1700 cm^{-1} spectral region, presented in Figure 7, where the results of irradiation at λ = 265 nm for 1 h are shown. In this figure, the calculated spectra of the proposed photoproducts (see Scheme 2) in the same spectral range are also shown for comparison. The observation that the changes in the intensities of the various new bands in the 2300−1700 cm^{-1} spectral range follow different patterns with time of irradiation indicates that these bands originate from different products.

For the interpretation of the photochemical results, it must be noticed that TSMT is a molecule composed of 25 atoms, 15 of them belonging to the rigid benzisothiazole ring. Thus, 39 of the 69 vibrational modes are related to this benzisothiazole ring. This ring is unaffected by irradiation under the experimental conditions used, which results in extensive overlap of the bands of TSMT with those of the photoproducts, complicating interpretation of the data. The strong overlap of the spectra of some of the proposed photoproducts with each other and with the spectrum of TSMT can be clearly noticed in Figure S3 in the Supporting Information, where the calculated infrared spectra for the relevant species are shown. As can be seen in that figure, such superposition is particularly noticeable in the case of the most intense bands appearing in the low-frequency spectral range (below 1700 cm^{-1}), where most of the bands due to the benzisothiazole moiety appear. However, the most characteristic bands of the photoproducts are observed in the 2300−1700 cm^{-1} spectral region, which is a clean spectroscopic

dx.doi.org/10.1021/jo502419u | J. Org. Chem. 2015, 80, 392−400

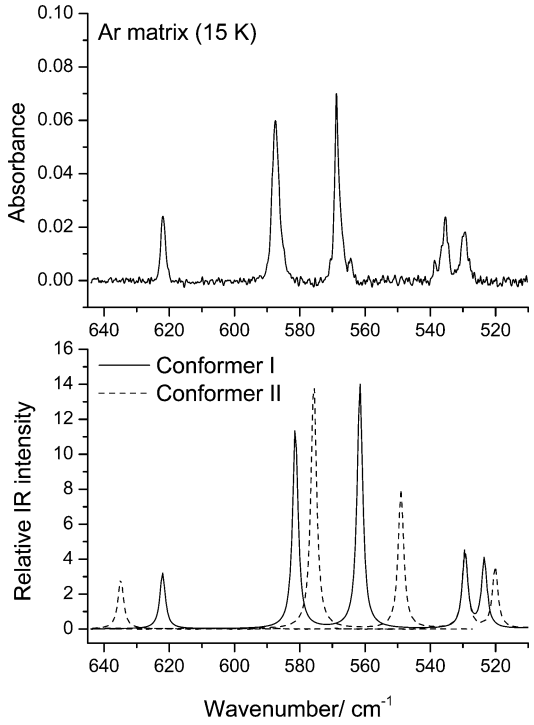

Figure 6. Low-frequency region of the infrared spectrum of matrix-isolated TSMT (Ar matrix, 15 K) and O3LYP/6-311++G(3df,3pd)-calculated infrared spectra of the two conformers of the compound in the same spectral range. The calculated spectra were simulated using Lorentzian functions centered at the calculated frequency scaled by 0.992 with fwhm equal to 2 cm^{-1}. It should also be noted that the peak intensities in the calculated spectrum differ from the calculated intensity values; in the figure the calculated intensities correspond to the areas of the peaks.

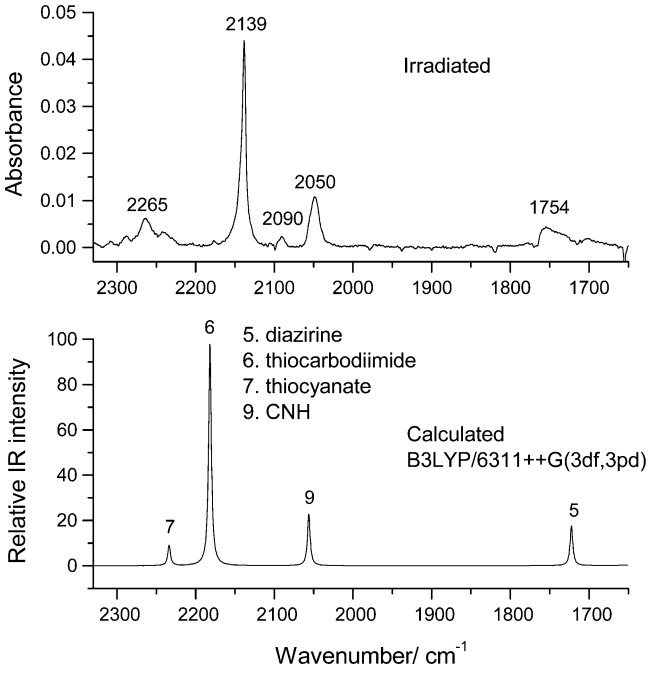

Figure 7. (top) IR spectrum in the 2300−1700 cm^{-1} spectral region for TSMT after irradiation of the matrix with UV light (λ = 265 nm) for 1 h, showing peaks due to the photolysis products. The peak at 1754 cm^{-1} is assigned to the N═C stretching vibration in diazirine **5**, the peak at 2139 cm^{-1} to the N═C═N antisymmetric stretching of thiocarbodiimide **6**, the peak at 2090 cm^{-1} to the N═N═N antisymmetric stretching of methyl azide (**8**), the peak at 2050 cm^{-1} to the CN stretching of CNH (**9**), and the peak at 2265 cm^{-1} to the C≡N stretching of thiocyanate **7**. (bottom) Theoretical spectra obtained for the observed photoproducts. The intensities of the individual spectra were multiplied by different factors to obtain a better simulation of the experimental spectrum. Theoretical wavenumbers were scaled by a factor of 0.978, and bands were broadened using Lorentzian functions with fwhm equal to 4 cm^{-1}.

window; this allowed us to doubtlessly identify these species, as described in detail below.

The band appearing at 2139 cm^{-1} (Figure 7) nicely fits the predicted frequency for the NCN antisymmetric stretching vibration of thiocarbodiimide **6** (Scheme 2). The observation of carbodiimides resulting from photolysis of matrix-isolated tetrazole derivatives has been reported previously.[28−30] Additionally, the bands appearing around 1754 cm^{-1} fit well the predicted frequencies for the $\nu_{C=N}$ stretching vibration of diazirine **5**. The formation of diazirines (including 1,3-substituted diazirines) from photochemically induced cleavage of the tetrazole ring has also been reported.[25,29]

The identification of bands assigned to thiocarbodiimide **6** and diazirine **5** suggests photocleavage of the N_{18}−N_{19} and N_{20}−N_{21} bonds (see Figure 2 for atom numbering) with extrusion of molecular nitrogen. It should be noted that the broad profile of the band around 1754 cm^{-1} may be due to the presence in the matrix of different conformers of diazirine **5**. Actually, this molecule has two rotational axes, S−$C_{(saccharin)}$ and S−$C_{(diazirine)}$, and calculations predicted the existence of two conformers with relative energies differing by only 2.9 kJ mol^{-1}. The two conformers have similar IR spectra, but the calculated frequencies for the $\nu_{C=N}$ mode are different enough (1722 and 1740 cm^{-1}) to result in the observed broad band.

It should also be noted that in the case of carbodiimide **6**, the calculated spectrum does not coincide so much with those of the reactant molecule and other photoproducts. As shown in Figure 8, several bands observed in the low-frequency range in the spectrum of the photolyzed matrix doubtlessly confirm this species as one of the dominant photoproducts of TSMT. Moreover, it should also be noticed that both carbodiimide **6** and diazirine **5** were formed from the very beginning of the irradiation, as they were already present in significant amounts after only 30 s of irradiation (see Figure 8).

The band observed at around 2100 cm^{-1} is likely due to methyl azide (**8**) (ν_{NNN} antisymmetric stretching), which can be formed by photocleavage of the N_{17}−N_{21} and N_{18}−N_{19} bonds of the tetrazole ring of TSMT upon irradiation, concomitant with thiocyanate **7**. Under the used irradiation conditions, **8** has been found to partially react to yield as the final main product CNH (**9**)[31] (together with H_2 and N_2) in a process where methylenimine (CH_2═NH) acts as an intermediate.[31−34] Indeed, the photochemistry of **8** in an argon matrix has been studied in the past and, for example, the production of radicals such as CN has been safely excluded.[32] According to the available knowledge on the photochemistry of **8**,[31−34] one can then expect that the formation of this compound from photolysis of TSMT should essentially result in the accumulation of CNH. In consonance with such expectations, a product band was observed around 2050 cm^{-1}, corresponding to the ν_{CN} stretching mode of CNH observed by Milligan and Jacox[31] upon photolysis of matrix-isolated **8** at nearly this frequency (2032 cm^{-1}). In the present study, CNH is formed together with other products and with

dx.doi.org/10.1021/jo502419u | J. Org. Chem. 2015, 80, 392−400

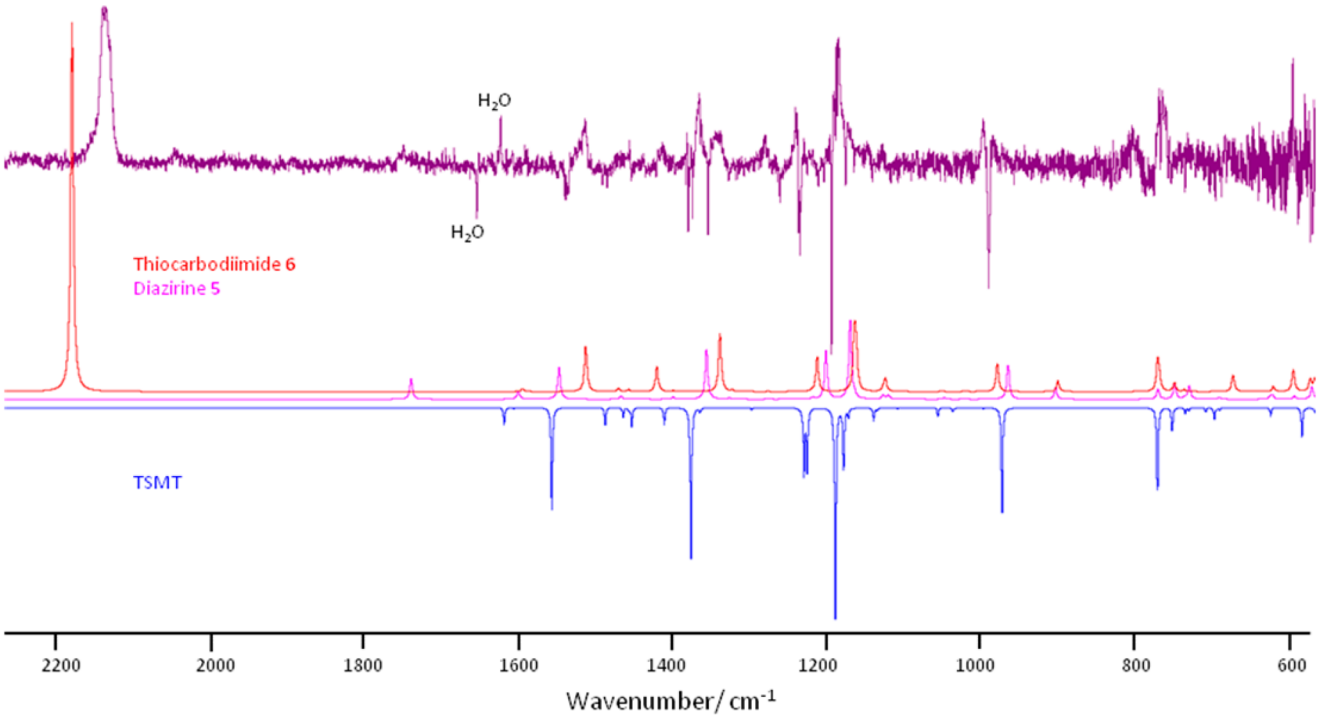

Figure 8. (top) Infrared difference spectrum (violet) obtained by subtracting the spectrum of the deposited TSMT matrix from that resulting from irradiation of the matrix (λ = 265 nm) for 30 s. (bottom) DFT-calculated (wavenumbers scaled) spectra for TSMT (blue trace, bands pointing down), thiocarboidiimide **6** (red trace), and diazirine **5** (magenta trace).

all probability interacts in the matrix cage with other species. Because of that, the frequencies may shift somewhat. Nevertheless, the assignment of the band at 2050 cm^{-1} to CNH seems to be doubtless. It is unfortunate that the other two additional bands due to CNH reported by Milligan and Jacox (at ca. 535 and 3583 cm^{-1})[31] could not be ascribed with certainty in the present study, though a product band at 536 cm^{-1} (almost coincident with a band of TSMT) seems also to be present in the spectrum of the photolyzed matrix. However, the large spectral noise below ca. 600 cm^{-1} in the spectrum of the photolyzed matrix makes this observation uncertain. On the other hand, the band observed by Milligan and Jacox[31] at 3583 cm^{-1} is due to the NH stretching mode of CNH and can be expected to be extensively broadened due to intermolecular interactions (hydrogen bonding) between CNH and other species present in the matrix cage (several bumps in the baseline are present in the spectrum of the photolyzed TSMT matrix in the high-frequency region; however, no band could be safely assign to this mode). It should also be noticed that no spectroscopic evidence of the presence of methylenimine in the photolyzed matrix could be found, specifically in the CH and C═N stretching spectral regions, where putative bands due to this compound appearing in a spectral region relatively less congested with bands due to other species should be observed. However, in the present experiments this species can be expected to be present only in very low amounts as a result of its expected prompt fragmentation into CNH and H_2,[31−34] and since its infrared spectrum is characterized by bands of very low intensity,[32] its successful observation would be very improbable.

The bands observed at around 2265 cm^{-1} correspond to typical frequencies of C≡N stretching modes[35,36] and can be assigned to the $\nu_{C\equiv N}$ vibrational mode of thiocyanate **7**, which is the photoproduct that can be expected to be formed together with **8** (see Scheme 2). The calculated intensity of this band for the thiocyanate in the gas phase is small, but it is possible that it intensifies to some extent in the matrix as a result of polarization effects induced by the medium. Very unfortunately, most of the other thiocyanate bands with significant predicted intensity are expected to be superimposed with bands due to diazirine **5** and TSMT (see Figure S3 in the Supporting Information). Since the direct evidence for the identification of thiocyanate **7** is mainly in the observation of the feature in the ∼2265 cm^{-1} region, it must be considered as tentative. However, this assignment is strongly suggested from the mechanistic point of view, since, as already mentioned, the thiocyanate is the product that can be expected to be formed simultaneously with methyl azide.

A schematic drawing that summarizes the proposed photochemistry of matrix-isolated TSMT is presented in Scheme 2. As mentioned above, according to the identified photoproducts, two photodegradation pathways can be postulated, both arising from cleavage of the tetrazolyl ring: the dominant pathway *a* involves photoinduced cleavage of the N_{18}−N_{19} and N_{20}−N_{21} bonds with extrusion of molecular nitrogen, leading to the production of diazirine **5** and thiocarbodiimide **6**. A nitrene-type intermediate can be postulated to be involved in this process,[28,29] though we could not experimentally observe it. The concentrations of both thiocarbodiimide **6** and diazirine **5** increased continuously with time, with no apparent sign of their further chemical transformations. The minor pathway *b* involves photoinduced cleavage of the C_{17}−N_{21} and N_{18}−N_{19} bonds of the tetrazole ring, leading to the formation of thiocyanate **7** and methyl azide; the thiocyanate remains photostable, while methyl azide undergoes subsequent decomposition into CNH.

An additional note shall here be made in relation to the observed photostability of diazirine **5**. The recent study by Nunes et al.[29] on the photolysis of the predominant 2*H*

dx.doi.org/10.1021/jo502419u | J. Org. Chem. 2015, 80, 392−400

Scheme 2. Proposed Reaction Pathways Resulting from Irradiation of TSMT Monomer Isolated in an Argon Matrix

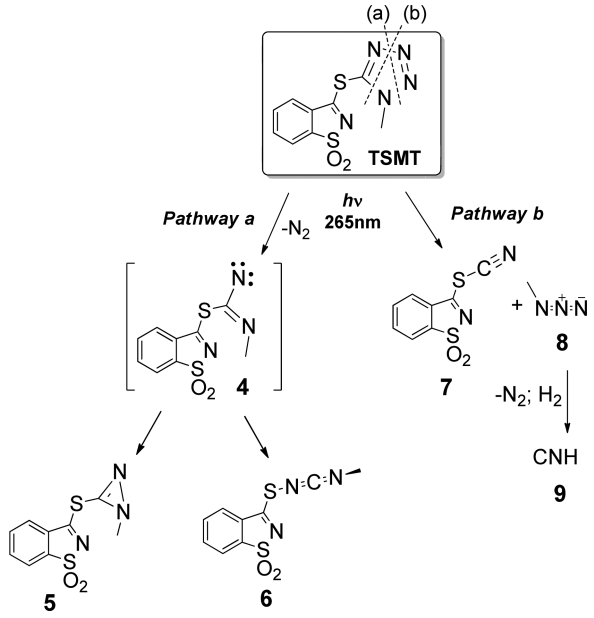

tautomeric form of matrix-isolated 5-methyltetrazole using light with λ = 222 and ~328 nm demonstrated that elimination of molecular nitrogen leads to the initial production of a nitrile imine after a few seconds of irradiation. This can then isomerize to a 1*H*-diazirine, which undergoes subsequent photoconversion into a carbodiimide. In the present work, no evidence for the formation of a nitrile imine was found, while the photoproduced diazirine was revealed to be photostable even after 1 h of irradiation (λ = 265 nm). This might indicate that the photochemistries of the 1*H* and 2*H* tautomers of substituted tetrazoles might be different, as suggested by Begué et al.[28] Indeed, the present results on TSMT should be compared more directly with those reported by the last authors[28] for 5-phenyl-1*H*-tetrazole, since TSMT is also a 1-substituted tetrazole derivative. Begué et al. observed that upon photolysis (λ = 254 nm) of 5-phenyl-1*H*-tetrazole, this tautomer did not produce the nitrile imine directly, contrary to what was observed for the 2*H* tautomer[28] (and also in the case of the 2*H* tautomer of 5-methyltetrazole,[29] as mentioned above). The suggested route for the production of the nitrile imine starting from the 1*H* tautomer of 5-phenyltetrazole considered by Begué et al. implies the initial production of a diazirine intermediate, despite the fact that they were not able to observe this species (see Scheme S1 in the Supporting Information).[28] The present observation of diazirine **5** as a stable photoproduct seems to confirm the proposition of Begué et al.[28] The photostability of **5** is probably due to both the stabilizing effect of the electron-rich sulfur substituent of the tetrazole ring and the presence of the methyl substituent, which preclude the photoinduced rearrangement of **5** under the experimental conditions used.

CONCLUSIONS

A combined matrix-isolation FTIR and theoretical study of the molecular structure and photochemistry of 5-thiosaccharyl-1-methyltetrazole was performed. The conformational preferences of TSMT in both the matrix-isolated situation and the crystalline phase were also investigated.

According to the performed DFT calculations, TSMT has two conformers, I and II. However, the higher-energy form, II, has a relative energy of ca. 15 kJ mol^{-1}, and only conformer I is significantly populated in the gas phase. As could be expected, this conformer was found to be the only one detectable in the cryomatrices (15 K) prepared from the vapor of the compound at 100 °C. The infrared spectrum of matrix-isolated TSMT was fully assigned on the basis of the O3LYP/6-311++G(3df,3pd) spectra calculated for conformer I.

In the crystal, TSMT was also found to exist in form I. In the crystalline phase, each molecule of TSMT forms four hydrogen bonds with three neighboring molecules, and a network of TSMT dimers is clearly observed. In the dimers, the two molecules of TSMT are disposed in a head-to-tail arrangement, with the tetrazole moiety of one molecule overlapping the thioimino moiety of the other (and vice versa) at the inner part of the dimer while the aromatic rings are directed to the extremities. The formation of dimers is possibly due to $\pi-\pi$ interactions between complementary tetrazole ring and thioimino moieties. The oligomeric structure results from an intricate network of weak hydrogen bonds formed between consecutive dimers (with involvement of both molecules of the dimer) and adjacent dimers.

Upon irradiation of the matrix-isolated compound with UV light (λ = 265 nm), two photodegradation pathways were observed, both arising from cleavage of the tetrazolyl ring: Pathway *a* involves photoinduced cleavage of the N_1-N_2 and N_3-N_4 bonds with extrusion of molecular nitrogen, leading to the production of diazirine **5** and thiocarbodiimide **6**. The concentrations of these two photoproducts increased with time, and there was no apparent sign of their photodegradation even after almost complete consumption of the reagent (TSMT). The observed photostability of the photoproduct diazirine **5** under the conditions used is possibly ascribable to a stabilizing effect of the electron-rich sulfur substituent and the presence of the 1-methyl substituent. Pathway *b* involves photoinduced cleavage of the C_5-N_1 and N_4-N_3 bonds, leading to thiocyanate **7** and methyl azide (**8**) as primary photoproducts. Thiocyanate **7** remains photostable while **8** forms CNH (**9**) in a secondary photoreaction.

EXPERIMENTAL SECTION

General Methods. A convergent synthetic approach was followed to prepare TSMT, as depicted in Scheme 1. Solvents for extraction were of technical grade. When required, solvents were freshly distilled from appropriate drying agents before use. Melting points were recorded and are uncorrected. Mass spectra were obtained by electron ionization (EI) at 70 eV. NMR (400 MHz) spectra were measured using TMS as the internal reference (δ = 0.0 ppm).

Preparation of 3-Chloro-1,2-benzisothiazole-1,1-dioxide. Saccharyl chloride (3-chloro-1,2-benzisothiazole-1,1-dioxide, **2**) was obtained by heating saccharin (10.2 g, 56 mmol) and phosphorus pentachloride (14.0 g, 66 mmol) at 180 °C using a procedure reported previously.[37] Colorless needles (7.00 g, 63% yield). ^{1}H NMR (400 MHz, $CDCl_3$): δ 7.95–7.82 (m, 4H). Elemental analysis: C 41.5%, H 2.0%, N 6.9% (found); C 41.7%, H 2.0%, N 7.0% (calculated for $C_7H_4NO_2SCl$).

Preparation of 1,2-Benzisothiazole-1,1-dioxo-3-(5-thio-1-methyl)tetrazole (TSMT). A mixture of anhydrous 5-mercapto-1-methyltetrazole (**1**) (0.30 g, 2.56 mmol) and 3-chloro-1,2-benzisothiazole-1,1-dioxide (**2**) (0.53 g, 2.56 mmol) in dry THF (20 mL) was stirred at 60 °C under a nitrogen atmosphere. The reaction was monitored by TLC (5:3 toluene/acetone). After 24 h, the solvent was evaporated under reduced pressure, and the remaining solid was dried under vacuum at room temperature. Crystallization from 2:1

dx.doi.org/10.1021/jo502419u | J. Org. Chem. 2015, 80, 392–400

chloroform/THF yielded the required product as colorless crystals (0.6 g, 83% yield), mp 222−224 °C. ^{1}H NMR (400 MHz, $CDCl_3$): δ 7.98−7.96 (m, 1H), 7.91−7.79 (m, 3H), 4.22 (s, 3H). ^{13}C NMR (101 MHz, $CDCl_3$): δ 170.35, 165.77, 139.44, 135.13, 134.35, 128.84, 123.34, 122.94, 35.26. MS (EI): m/z 281 $[M]^+$.

Matrix Preparation, Infrared Spectroscopy, and Irradiation Experiments. The matrix was prepared by codeposition of the matrix gas (argon, 99.9998%, obtained from Air Liquid) and vapors of TSMT produced by sublimation onto the cooled CsI substrate of the cryostat in a specially designed variable-temperature mini-oven assembled inside the cryostat. The temperature of the mini-oven used for sublimation of TSMT was ca. 100 °C. The cryogenic system was based on a closed-cycle helium refrigeration system with a DE-202A expander. The temperature of the CsI substrate during deposition was 15 K.

The infrared spectrum of matrix-isolated TSMT was obtained using a Fourier transform infrared spectrometer equipped with a deuterated triglycinesulfate (DTGS) detector and a Ge/KBr beam splitter with 0.5 cm^{-1} spectral resolution. The room-temperature IR spectrum (4000−400 cm^{-1}) of solid polycrystalline TSMT in a KBr pellet was obtained using a Fourier transform spectrometer equipped with a DTGS detector and Zn/Se optics. Data collection was performed with 128 scans and 4 cm^{-1} spectral resolution.

The matrix was irradiated through the outer quartz window of the cryostat with the frequency-doubled signal beam of a Quanta-Ray MOPO-SL pulsed (10 ns) optical parametric oscillator (fwhm ∼0.2 cm^{-1}, repetition rate 10 Hz, pulse energy ∼5.8 mJ) pumped with a pulsed Nd:YAG laser.

Crystallographic Analysis. X-ray diffraction data were collected using a small single crystal. The crystallographic structure was solved by direct methods using SHELXS-97.[38] Refinements were carried out with the SHELXL-97 package.[39] All refinements were made by full-matrix least-squares on F^2 with anisotropic displacement parameters for all non-hydrogen atoms (see Table S3 in the Supporting Information for details). All of the hydrogen atoms could be located on a difference Fourier synthesis; their positions were refined as riding on parent atoms with isotropic temperature factors using SHELXL-97 defaults that constrain these atoms to idealized positions. X-ray data collection and processing parameters for TSMT are presented in Table S3.

Computational Methods. Quantum-chemical calculations were performed with density functional theory using either the valence double-ζ polarized 6-31++G(d,p) or extended-valence triple-ζ polarized 6-311++G(3df,3pd) basis set[40−43] and the B3LYP or O3LYP functional.[44,45] Inclusion of both diffuse and polarization functions in the basis sets was required for a more accurate approximation of the calculated infrared spectra, since vibrational modes involving hypervalent S atoms (in particular the $>SO_2$ stretching and bending modes) are known not to be correctly predicted at a lower level of approximation.[46,47] The use of the B3LYP or O3LYP functional with the 6-311++G(3df,3dp) basis set was found to be appropriate to attain reliable results with moderate computational effort.[12,13,46,47] Geometries were optimized using the direct inversion in the iterative subspace (DIIS) method.[48] The transition state was located using the synchronous-transit quasi-Newton method (QST3 implementation).[49,50] The optimization of geometries was followed by harmonic vibrational calculations undertaken at the same level of theory. The nature of the obtained stationary points was checked through analysis of the corresponding Hessian matrix. The calculated harmonic vibrational frequencies (scaled by the factor 0.978 for the B3LYP functional[51] and by the factor 0.992 for the O3LYP functional[13]) were used to assist the analysis of the experimental spectra. All of the calculations were performed with the Gaussian 09 suite of programs.[52]

■ ASSOCIATED CONTENT

Supporting Information

^{1}H and ^{13}C NMR spectra of TSMT; IR spectrum of the TSMT crystal and calculated IR spectra of TSMT and relevant photoproducts; tables of experimental (X-ray, single-crystal) details of the crystallographic studies and calculated geometrical parameters of TSMT, including Cartesian coordinates, electronic energies, and calculated infrared spectra for all optimized structures at the B3LYP/6-311++G(3df,3pd) and O3LYP/6-311++G(3df,3pd) levels; and crystallographic data in CIF format. This material is available free of charge via the Internet at http://pubs.acs.org.

■ AUTHOR INFORMATION

Corresponding Authors

*E-mail: mcristi@ualg.pt.

*E-mail: rfausto@ci.uc.pt.

Notes

The authors declare no competing financial interest.

■ ACKNOWLEDGMENTS

The authors gratefully acknowledge Fundação para a Ciência e a Tecnologia (FCT), Portugal (Project PEst-C/MAR/LA0015/2013), cofunded by QREN-COMPETE-UE, and CCMAR for generous financial support. The Coimbra Chemistry Centre (CQC) and CEMDRX are also supported by FCT through Projects PEst-OE/QUI/UI0313/2014 and PEst-OE/FIS/UI0036/2014, respectively. A.I. acknowledges FCT for the award of a doctoral grant (SFRH/BD/90435/2012). A.B. acknowledges FCT for the award of a postdoctoral grant (SFRH/BPD/66154/2009).

■ REFERENCES

(1) Zhao, H.; Qu, Z.-R. R.; Ye, H.-Y. Y.; Xiong, R.-G. G. *Chem. Soc. Rev.* **2008**, *37*, 84−100.

(2) Baran, E. J.; Yilmaz, V. T. *Coord. Chem. Rev.* **2006**, *250*, 1980−1999.

(3) Abu-Youssef, M. A. M.; Mautner, F. A.; Massoud, A. A.; Öhrström, L. *Polyhedron* **2007**, *26*, 1531−1540.

(4) Xiong, R.-G.; Xue, X.; Zhao, H.; You, X.-Z.; Abrahams, B. F.; Xue, Z. *Angew. Chem., Int. Ed.* **2002**, *41*, 3800−3803.

(5) Kim, Y.-J.; Joo, Y.-S.; Han, J.-T.; Han, W. S.; Lee, S. W. *J. Chem. Soc., Dalton Trans.* **2002**, 3611−3618.

(6) Gupta, A. K.; Song, C. H.; Oh, C. H. *Tetrahedron Lett.* **2004**, *45*, 4113−4116.

(7) Naumov, P.; Jovanovski, G. *Struct. Chem.* **2000**, *11*, 19−33.

(8) Cotton, F. A.; Falvello, L. R.; Schwotzer, W.; Murillo, C. A.; Valle-Bourrouet, G. *Inorg. Chim. Acta* **1991**, *190*, 89−95.

(9) Jovanovski, G.; Hergold-Brundić, A.; Grupče, O.; Matković-Čalogović, D. *J. Chem. Crystallogr.* **1999**, *29*, 233−237.

(10) Frija, L. M. T. T.; Fausto, R.; Loureiro, R. M. S. S.; Cristiano, M. L. S. *J. Mol. Catal. A: Chem.* **2009**, *305*, 142−146.

(11) Gómez-Zavaglia, A.; Ismael, A.; Cabral, L. I. L.; Kaczor, A.; Paixão, J. A.; Fausto, R.; Cristiano, M. L. S. *J. Mol. Struct.* **2011**, *1003*, 103−110.

(12) Ismael, A.; Gómez-Zavaglia, A.; Borba, A.; Cristiano, M. d. L. S.; Fausto, R. *J. Phys. Chem. A* **2013**, *117*, 3190−3197.

(13) Duarte, L.; Reva, I.; Cristiano, M. d. L. S.; Fausto, R. *J. Org. Chem.* **2013**, *78*, 3271−3275.

(14) Kamigata, N.; Saegusa, T.; Fujie, S.; Kobayashi, M. *Chem. Lett.* **1979**, 9−12.

(15) Ono, I.; Sato, S.; Fukuda, K.; Inayoshi, T. *Bull. Chem. Soc. Jpn.* **1997**, *70*, 2051−2055.

(16) Lancaster, M.; Smith, D. J. H. *J. Chem. Soc., Chem. Commun.* **1980**, 471.

(17) Dietrich, D. *Int. J. Photoenergy* **2001**, *3*, 41−48.

(18) Elghamry, I.; Dopp, D. *Tetrahedron Lett.* **2001**, *42*, 5651−5653.

(19) Dopp, D.; Lauterfeld, P.; Schneider, M.; Schneider, D.; Henkel, G.; Issac, Y.; Elghamry, I. *Synthesis* **2001**, 1228−1235.

(20) Elghamry, I.; Dopp, D.; Henkel, G. *J. Heterocycl. Chem.* **2007**, *44*, 849−852.
(21) Western, A.; Van Camp, J. R.; Bensasson, R.; Land, E. J.; Kochevar, I. E. *Photochem. Photobiol.* **1987**, *46*, 469−475.
(22) Miranda, M. A.; Vargas, F.; Serrano, G. *J. Photochem. Photobiol., B* **1991**, *8*, 199−202.
(23) Cho, D. W.; Oh, S. W.; Kim, D. U.; Park, H. J.; Xue, J. Y.; Yoon, U. C.; Mariano, P. S. *Bull. Korean Chem. Soc.* **2010**, *31*, 2453−2458.
(24) Frija, L. M. T.; Ismael, A.; Cristiano, M. L. S. *Molecules* **2010**, *15*, 3757−3774.
(25) Frija, L. M. T.; Cristiano, M. L. S.; Gómez-Zavaglia, A.; Reva, I.; Fausto, R. *J. Photochem. Photobiol., C* **2014**, *18*, 71−90.
(26) Ismael, A.; Cristiano, M. L. S.; Fausto, R.; Gómez-Zavaglia, A. *J. Phys. Chem. A* **2010**, *114*, 13076−13085.
(27) Belaidi, O.; Bouchaour, T.; Maschkle, U. *Org. Chem. Int.* **2013**, No. 384520.
(28) Bégué, D.; Qiao, G. G.; Wentrup, C. *J. Am. Chem. Soc.* **2012**, *134*, 5339−5350.
(29) Nunes, C. M.; Araujo-Andrade, C.; Fausto, R.; Reva, I. *J. Org. Chem.* **2014**, *79*, 3641−3646.
(30) Pagacz-Kostrzewa, M.; Mucha, M.; Weselski, M.; Wierzejewska, M. *J. Photochem. Photobiol., A* **2013**, *251*, 118−127.
(31) Milligan, D. E.; Jacox, M. E. *J. Chem. Phys.* **1963**, *39*, 712−715.
(32) Milligan, D. E. *J. Chem. Phys.* **1961**, *35*, 1491−1497.
(33) Nguyen, M. T. *Chem. Phys. Lett.* **1985**, *117*, 290−294.
(34) Nguyen, M. T.; Sengupta, D.; Ha, T.-K. *J. Phys. Chem.* **1996**, *100*, 6499−6503.
(35) Schrader, B. *Infrared and Raman Spectroscopy: Methods and Applications*; VCH: Weinheim, Germany, 1995.
(36) Chalmers, J. M.; Griffiths, P. R. Spectra−Structure Correlations in the Mid- and Far-Infrared. In *Handbook of Vibrational Spectroscopy*; Wiley: Chichester, U.K., 2001.
(37) Vogel, A. I.; Tatchell, A. R.; Furnis, B. S.; Hannaford, A. J.; Smith, P. W. G. *Vogel's Textbook of Practical Organic Chemistry*, 5th ed.; Longman: London, 1989; p 881.
(38) Sheldrick, G. M. *SHELXS-97: Program for the Solution of Crystal Structure*, 1997.
(39) Sheldrick, G. M. *SHELXL-97: Program for the Refinement of Crystal Structure*, 1997.
(40) Krishnan, R.; Binkley, J. S.; Seeger, R.; Pople, J. A. *J. Chem. Phys.* **1980**, *72*, 650−654.
(41) McLean, A. D.; Chandler, G. S. *J. Chem. Phys.* **1980**, *72*, 5639−5648.
(42) Frisch, M. J.; Pople, J. A.; Binkley, J. S. *J. Chem. Phys.* **1984**, *80*, 3265−3269.
(43) Clark, T.; Chandrasekhar, J.; Spitznagel, G. W.; Schleyer, P. v. R. *J. Comput. Chem.* **1983**, *4*, 294−301.
(44) Gill, P. M. W.; Johnson, B. G.; Pople, J. A.; Frisch, M. J. *Chem. Phys. Lett.* **1992**, *197*, 499−505.
(45) Becke, A. D. *Phys. Rev. A* **1988**, *38*, 3098−3100.
(46) Kaczor, A.; Almeida, R.; Gómez-Zavaglia, A.; Cristiano, M. D. S.; Fausto, R. *J. Mol. Struct.* **2008**, *876*, 77−85.
(47) Almeida, R.; Gómez-Zavaglia, A.; Kaczor, A.; Ismael, A.; Cristiano, M. L. S.; Fausto, R.; Gómez-Zavaglia, A. *J. Mol. Struct.* **2009**, *938*, 198−206.
(48) Pulay, P. *J. Comput. Chem.* **1982**, *3*, 556−560.
(49) Peng, C.; Schlegel, H. B. *Isr. J. Chem.* **1993**, *33*, 449−454.
(50) Peng, C.; Ayala, P. Y.; Schlegel, H. B.; Frisch, M. J. *J. Comput. Chem.* **1996**, *17*, 49−56.
(51) Andrzejewska, A.; Lapinski, L.; Reva, I.; Fausto, R. *Phys. Chem. Chem. Phys.* **2002**, *4*, 3289−3296.
(52) Frisch, M. J.; Trucks, G. W.; Schlegel, H. B.; Scuseria, G. E.; Robb, M. A.; Cheeseman, J. R.; Scalmani, G.; Barone, V.; Mennucci, B.; Petersson, G. A.; Nakatsuji, H.; Caricato, M.; Li, X.; Hratchian, H. P.; Izmaylov, A. F.; Bloino, J.; Zheng, G.; Sonnenberg, J. L.; Hada, M.; Ehara, M.; Toyota, K.; Fukuda, R.; Hasegawa, J.; Ishida, M.; Nakajima, T.; Honda, Y.; Kitao, O.; Nakai, H.; Vreven, T.; Montgomery, J. A., Jr.; Peralta, J. E.; Ogliaro, F.; Bearpark, M.; Heyd, J. J.; Brothers, E.; Kudin, K. N.; Staroverov, V. N.; Kobayashi, R.; Normand, J.; Raghavachari, K.; Rendell, A.; Burant, J. C.; Iyengar, S. S.; Tomasi, J.; Cossi, M.; Rega, N.; Millam, J. M.; Klene, M.; Knox, J. E.; Cross, J. B.; Bakken, V.; Adamo, C.; Jaramillo, J.; Gomperts, R.; Stratmann, R. E.; Yazyev, O.; Austin, A. J.; Cammi, R.; Pomelli, C.; Ochterski, J. W.; Martin, R. L.; Morokuma, K.; Zakrzewski, V. G.; Voth, G. A.; Salvador, P.; Dannenberg, J. J.; Dapprich, S.; Daniels, A. D.; Farkas, Ö.; Foresman, J. B.; Ortiz, J. V.; Cioslowski, J.; Fox, D. J. *Gaussian 09*, revision A.02; Gaussian, Inc.: Wallingford, CT, 2009.